Published in final edited form as:
Matrix Biol. 2008 January ; 27(1): 53–66.

Increased degradation of extracellular matrix structures of lacrimal glands implicated in the pathogenesis of Sjögren's syndrome

Katja Schenke-Layland[1,#,§], **Jiansong Xie**[2,§], **Ekaterini Angelis**[1], **Barry Starcher**[3], **Kaijin Wu**[2], **Iris Riemann**[4], **W. Robb MacLellan**[1], and **Sarah F. Hamm-Alvarez**[2]

1*Cardiovascular Research Laboratory, David Geffen School of Medicine at UCLA, Los Angeles/CA, USA*

2*Department of Pharmacology and Pharmaceutical Sciences, School of Pharmacy, USC, Los Angeles/CA, USA*

3*Department of Biochemistry, University of Texas Health Center, Tyler/TX, USA*

4*Fraunhofer Institute of Biomedical Technology (IBMT), St. Ingbert, Germany*

Abstract

Lacrimal glands (LGs) of male non-obese diabetic (NOD) mice display many features of human LGs in patients afflicted with the autoimmune disease Sjögren's syndrome (SS), including the loss of secretory functions and a lymphocytic infiltration into the glands by 4 months of age. So far, research has mainly focused on the intracellular events that are involved in initiating LG dysfunction; however, the impact of SS on extracellular matrix (ECM) structures of the diseased LGs has not yet been determined. In this study we identified and compared LG ECM formation and integrity of age-matched male healthy (BALB/c) and diseased (NOD) mice. LG tissues were examined using routine histological, biochemical, immunohistochemical and gene expression analysis. Multiphoton imaging and second-harmonic generation (SHG) microscopy permitted the non-invasive analysis of major LG ECM structures including collagen- and elastin-containing fibers. Biochemical testing demonstrated a significant loss of collagen, glycosaminoglycans and desmosine in NOD-LGs when compared to healthy BALB/c-LGs. Immunohistochemical staining and gene expression analysis confirmed this disease-related alteration of LG ECM structures. Furthermore, laser-induced autofluorescence and SHG microscopy revealed dramatic changes in the structural organization of most collagenous and elastic fibers of the diseased LG tissues that were more pronounced than those displayed by histological analysis. Our results clearly show an enhanced degradation of ECM proteins accompanied by the severe disorganization and deformation of ECM structures of diseased LG tissues. These new insights into the involvement of ECM degradation in SS may lead to novel therapies for patients suffering from dry eye disease.

Keywords

lacrimal gland; Sjögren's syndrome; collagen; elastin; extracellular matrix; multiphoton imaging

#Corresponding Author: Katja Schenke-Layland, Ph.D., University of California Los Angeles (UCLA), Cardiovascular Research Laboratory, 675 Charles E. Young Drive South, MRL 3-579, Los Angeles, CA 90095-1760, -USA-, Phone: (001) 310-206-6477; Fax: (001) 310-206-5777, E-mail: kschenkelayland@mednet.ucla.edu.
§These authors have contributed equally to this study.

1. Introduction

Sjögren's syndrome (SS) is characterized by three major symptoms: arthritis, dry mouth and dry eye, as originally described by Sjögren in 1933 (Sjögren, 1933). So far it has been shown that lymphocytes infiltrate lacrimal glands (LGs) and salivary glands (SGs), and that this infiltration is associated with atrophy and ultimately destruction of the glands (Fox et al., 1983; Fox, et al., 1986; Matsumoto et al., 1996), resulting in the severe dry eye and dry mouth that are SS patients' major symptoms. Because the LGs are seriously affected, patients cannot produce reflex tears, resulting in severe damage to the ocular surface including squamous metaplasia of the ocular surface epithelium, pain, corneal scarring and in severe cases, blindness (Tsubota et al., 1996). The precise mechanisms which trigger initiation of disease and that result in inflammatory infiltration of the LGs are still unknown, although various studies have speculated that alterations in intracellular signaling processes and/or alterations in intracellular trafficking processes are potential culprits (Tsubota et al., 2001; Ohlsson et al., 2002; Qian et al., 2003; Qian et al., 2004; Rose et al., 2005; da Costa et al., 2006).

Much of the fundamental architecture and functional properties of the SG are dictated by its relationship with the underlying extracellular matrix (ECM). The ECM provides a substrate for attachment of the acinar epithelial cells within the gland, while providing signaling cues that trigger selective development and differentiation in response to pressures such as cell loss due to necrosis or apoptosis. In fact, the aberrant processing of ECM including the degradation of biglycan, decorin and collagen (Yamachika et al., 2000; Molina et al., 2005) and the elevated expression of MMPs in the SGs (Konttinen et al., 1998; Goicovich et al., 2003; Kontinnen et al., 1994; Perez et al., 2005) have been implicated as possible contributors to the altered glandular function that gives rise to SS in this organ. Given the structural and functional similarity of LGs to SGs, one might expect that the ECM plays a critical role in LG development and function, and that changes in the ECM might exert pathogenic effects. However, until now the changes in the ECM that accompany SS in the LG have not been characterized.

The non-obese diabetic (NOD) mouse represents a naturally-occurring model of SS and has been widely utilized to investigate many aspects of SS development and progression (Robinson et al., 1997; Yamachika et al., 1998; Humphreys-Beher and Peck, 1999; da Costa et al., 2006). In addition to the development of lymphocytic infiltration within the islets of Langerhans, the initiating event in the autoimmune diabetes that is well-established within this strain, these mice exhibit a lymphocytic infiltration into LGs and SGs, an effect accompanied by secretory dysfunction of these organs (da Costa et al., 2006). This effect in the male mice, which exhibit the most severe LG disease in this animal model, has an onset of 6-10 weeks while the clinical signs of disease are detectable by 4 months of age. Interestingly, the development of diabetes proceeds independently of SS-like symptoms in these mice.

In this study, we have examined the changes in LG ECM from male NOD mice and age-matched control BALB/c mice, focusing on events that occur by 18 weeks of age when inflammatory infiltration into the LGs is seen in almost all animals. We provide evidence that ECM undergoes dramatic changes in concert with the development of SS-like symptoms including degradation of collagen and elastin fibrils. Intriguingly, our data show that these changes are partly attributable to the altered expression of ECM constituent proteins within the acinar cells that make up the bulk of the LG, and also partly attributable to an increased MMP activity within the LGs.

2. Results

2.1. Morphological and microscopic analysis of LG tissues

Macroscopic visualization revealed dramatic differences between age-matched healthy (BALB/c) and diseased (NOD) LG tissues (Fig. 1). Compared to BALB/c LG specimens (Fig. 1A, C), NOD LGs (Fig. 1B, D) showed a significant increase in size, accompanied by the development of a spongy, degenerated histoarchitecture.

Routine histological analysis demonstrated an infiltration of mononuclear inflammatory cells into the glandular parenchyma, predominantly around acini and ducts, starting at the age of 7 weeks, which was further increased as the animals aged (Fig. 2A). Movat-pentachrome and Hart's stain visualized major ECM components including collagen, elastin and glycosaminoglycans (GAG) (Fig. 2B and C). Compared to BALB/c LGs, NOD LGs showed less collagenous and elastic structures, accompanied by deteriorated and disrupted tissue morphology. Moreover, in NOD LG tissues, the number of ducts and blood vessels was decreased. The remaining detectable ducts and blood vessels appeared to be dilated (Fig. 2C, c and d).

2.2. Biochemistry and immunohistochemistry reveal changes in ECM protein expression in NOD LGs

Quantitative ECM analysis, summarized in Fig. 3, showed in contrast with BALB/c LG tissues significantly decreased amounts of major ECM proteins in NOD LGs including collagen, glycosaminoglycans and desmosine, an amino acid cross-link specific to elastin. Specifically, the GAG content of BALB/c tissues was 5.1 ± 1.6 μg/mg wet weight, compared to 2.6 ± 0.6 μg/mg wet weight GAG in NOD LGs. The mean total collagen content of BALB/c tissues was 39.1 ± 4.8 μg/mg wet weight, compared to a significantly lower value of 12.3 ± 1.9 μg/mg wet weight in NOD LGs (Fig. 3A). The desmosine content in BALB/c LG tissues was detected as 20 ± 5 pm/mg total protein, whereas the mean desmosine content of NOD LGs was 14 ± 2 pm/mg total protein (Fig. 3B).

Dramatic changes of LG ECM structures and patterns in BALB/c versus NOD mice were further confirmed by immunohistochemical staining using antibodies against fibronectin (Fig. 4 A, B); collagen type I (Fig. 4 C, D); collagen type III (Fig. 4 E, F); collagen type IV (Fig. 4 G, H); laminin 1 (Fig. 4 I, J); heparan-sulphated-GAG (HS-GAG) (Fig. 4 K, L); decorin (Fig. 4 M, N); and tropoelastin (Fig. 4 O, P). In healthy control BALB/c tissues, clear expression patterns of those ECM proteins were observable. Briefly, fibronectin was weakly expressed in the acini, moderately expressed in the ducts, and was strongly detectable in the blood vessels (Table 1 and Fig. 4 A). Collagen types I and IV, laminin 1, as well as HS-GAG were moderately to strongly expressed in the basement membranes of acini and blood vessels, with a weaker expression around the ducts (Table 1 and Fig. 4 C, G, I, K). Collagen type III was predominantly expressed around the ducts, with a weaker expression in the basement membranes of acini and blood vessels (Table 1 and Fig. 4E). Decorin was moderately expressed throughout the whole tissue, surrounding all structures including acini, ducts and blood vessels (Table 1 and Fig. 4M). Expression of tropoelastin was not observable within or around the acini, but was weakly detected in blood vessels, and strongly expressed in the ducts (Table 1 and Fig. 4O). In contrast, immunohistochemical staining of NOD LG tissue sections revealed severe changes in LG ECM protein expression patterns (Table 1 and Fig. 4 D, F, H, J, L, N, P). These changes, manifested by an excessive degradation of matrix proteins, visible as zones of very poor immunofluorescence reactivity, were predominantly found in areas that showed elevated levels of inflammatory infiltrates. The most affected LG structures were the acini, with no expression of collagen type I, collagen type III and laminin 1, a very weak expression of collagen type IV and HS-GAG, and a weak expression of decorin (Table 1 and Fig. 4 D, F, H, J, L, N).

Differences were also found in the ducts, showing a weaker expression of collagen types I and III, decorin and tropoelastin (Table 1 and Fig. 4 D, F, N, P). Similar to previous studies on salivary glands from patients afflicted with Sjögren's syndrome (Goicovich et al., 2003; Molina et al., 2006), we found that the changes in ECM protein expression patterns were predominantly observable in the gland parenchyma, whereas changes to the basal lamina of blood vessels were absent. Furthermore, only minor changes were noted in the expression of decorin and tropoelastin (Table 1 and Fig. 4 N, P). Interestingly, within the same NOD LG tissue there were both areas with intense inflammatory cell infiltration, associated with a disorganized basal lamina, as well as areas free of inflammatory cells in which the basal lamina had a normal appearance (Fig. 4H). No apparent differences in the expression pattern of fibronectin were detectable (Table 1 and Fig. 4B).

2.3. Gene expression analysis and gelatinase activity

Microarray analysis showed a more than 1.5-fold down-regulation of major ECM genes, including collagens type I, III and IV, as well as of laminin 1 in NOD LG tissues when compared to LG samples from BALB/c mice (data not shown). To further confirm those data we performed semi-quantitative and quantitative RT-PCR. Semi-quantitative RT-PCR results showed a down-regulation of collagen type I (Col1a1, Col1a2), type III (Col3a1) and type IV (Col4a1), laminin 1 (Lama1) as well as decorin (Dcn), and an up-regulation of tenascin C (Tnc) in NOD LG tissues compared to BALB/c LGs (Fig. 5A). No significant changes in the expression of elastin were observed (Fig. 5A).

To quantify these results we performed real-time PCR (Fig. 5B). GAPDH as well as Rab3d served as internal controls. Rab3d is a marker that has been shown to be specific to lacrimal acinar epithelial cells (Schlüter et al., 2002), but is not expressed in inflammatory cells. Semi-quantitative RT-PCR revealed that there is no significant difference in Rab3d expression in BALB/c and NOD LGs, relative to GAPDH (Fig. 5B). Using GAPDH for normalization, we found a significant up-regulation of tenascin C by 52%, and a down-regulation of collagen type I by 58%-65%, collagen type III by 73%, collagen type IV by 67%, laminin 1 by 78% and decorin by 46% in NOD LGs (Fig. 5B). Interestingly, when using Rab3d for normalization (to exclude that the reduced ECM gene expression is rather due to a dilution of acinar-cell-RNA by the inflammatory-cell-RNA than by an actual down-regulation of ECM gene expression within the acinar cells), we still found a modest down-regulation of most of the ECM genes; however, this down-regulation was, except for collagen type IV not statistically significant (Fig. 5B). Furthermore, the expression of elastin and especially tenascin C was significantly increased in NOD LG samples when compared to BALB/c LGs utilizing either marker (Fig. 5B). Tenascin C is an important ECM glycoprotein expressed in a spatiotemporally restricted pattern associated with tissue remodeling during embryonic development (heart and blood vessel development), wound healing, cancer invasion and tissue regeneration (Imanaka-Yoshida et al., 2003). Its distribution is restricted in normal adult tissues but it is up-regulated in tumors and under inflammatory conditions (Kostianovsky et al., 1997). Moreover, previous *in vitro* studies revealed that elevated levels of MMP activity in cultures of vascular smooth muscle cells could also induce expression of the Tnc (Cowan et al., 2000). To investigate if this finding is also true for the LG tissues of NOD mice, and to demonstrate if there is a relationship between the severe inflammatory infiltration of the NOD LGs and ECM degradation involving MMPs, we performed immunohistochemical staining and determined MMP2 and MMP9 activity levels using a gelatinase activity assay (Fig. 5C and D). Immunohistochemistry showed a strong expression of MMP2 and MMP9 in areas of infiltration in NOD LGs, predominantly located around inflammatory cells including macrophages, their precursors and T lymphocytes that were identified using antibodies against CD11b (data not shown), CD4 and CD68 (Fig. 5C e-h). Staining of the non-infiltrated BALB/c LGs showed no or only weak expression of MMP2 and MMP9 (Fig. 5C a-d). The gelatinase

activity assay, which utilizes a biotinylated gelatinase substrate that is cleaved by active MMP2 and MMP9, confirmed the results obtained by immunohistochemical staining, showing a statistically significant increase of MMP2 and MMP9 activity in NOD LGs when compared to BALB LGs (Fig. 5D).

2.4. Fluorescence-activated cell sorter (FACS) analysis of inflammatory infiltrates

In order to better characterize the NOD LG inflammatory infiltrates, FACS analysis was performed revealing the presence of various populations of macrophages, neutrophilic and eosinophilic granulocytes, B- and T-cells (Fig. 6 A-C). In detail, double-staining using antibodies against CD11b and GR1 showed that approximately 43% of the inflammatory cells are macrophages (CD11b+ GR1-), 6% of the cells represent CD11b+ GR1+ myeloid immunoregulatory cells (consisting of $CD11b^{low}$ GR1 and $CD11b^{high}$ GR1 subsets), and 4.5% are of granulocytic origin (CD11b- GR1+) (Kusmartsev, et al., 2000; Maruyama et al., 2005) (Fig. 6A). Double-labeling using antibodies against B220 and CD19 revealed the presence of two major B-cell populations: 4.8% B220+ CD19- and 54% B220+ CD19+ B lymphoid progenitor cells (Ogawa et al., 2000) (Fig. 6B). Further staining using antibodies against CD4 and CD8 demonstrated 8.8% CD8+ CD4- (mature cytotoxic T cells) cells, 4.5% CD8+ CD4+ (immature T cells), and 15% CD8-CD4+ cells (mature T helper cells) (Matsumoto et al., 1996; Germain RN, 2002) (Fig. 6C).

2.5. Multiphoton-induced autofluorescence and SHG imaging

Tissue state and quality of ECM structures including collagen bundles and elastin-containing fibers of BALB/c and NOD LG tissues were assessed using non-destructive multiphoton-induced autofluorescence microscopy and SHG imaging (Figs. 7 and 8). To visualize intra-tissue ECM structures via their native autofluorescent properties, wavelengths of 740 nm (cells and elastic fibers) and 860 nm (collagen fibers) were determined as appropriate excitation wavelengths (Fig. 7A). Exposure of fresh dissected BALB/c LG tissues to laser pulses at 740 nm revealed cellular structures (acinar cells) and a few elastic fibers within tissue depths of 20 to 30 μm (Fig. 7A, a, e and Fig. 7B). Using an excitation wavelength of 860 nm, wavy bundles of collagen were detectable in BALB/c LG specimens (Fig. 7A, c, e and Fig. 7B). In contrast, using a wavelength of 740 nm and similar or even higher laser powers as used for monitoring BALB/c tissues almost no autofluorescent cellular structures or elastic fibers were detectable in NOD tissues (Fig. 7A, b, f and Fig. 7B). Only with higher laser powers at a wavelength of 840 nm comparable autofluorescent collagen-containing structures were visualizable in NOD LG tissues (Fig. 7A, d, f and Fig. 7B).

When ECM components such as collagenous and elastic fibers loose their native pattern within a tissue they generate less detectable autofluorescence and SHG signals. Thus, diminished intrinsic fluorescence signal intensities are indicative of structural changes. The weaker the autofluorescence and SHG signal, the stronger is the evidence that major changes of the ECM structures have occurred. To quantitatively evaluate these changes in autofluorescence and SHG patterning we compared BALB/c and NOD LG ECM structures using spectral fingerprinting (Fig. 8). Applying this novel technique, using the same laser powers for all tissues, we were able to detect significant differences of intrinsic fluorescence signal intensity values (detected as gray value intensities (GVI)) of BALB/c (Fig. 8A, B) and NOD (Fig. 8 C, D) LG tissues. Accordingly, the autofluorescence and SHG signal intensities of elastic fibers and collagen-containing structures in BALB/c LGs were significantly higher (139 ± 2 GVI (collagen; ROI1) and 55 ± 5 GVI (elastin; ROI2)) when compared to NOD tissues (39 ± 3 GVI (collagen; ROI1) and 16 ± 4 GVI (elastin; ROI2)). The magnitude of the loss of elastin and collagen detected by this method appeared greater than the loss detected by standard histochemical labeling (Fig. 2), suggesting that some of structures labeled by standard methods might already be deteriorated or degraded.

3. Discussion

The ECM is a complex structural entity composed of fibrillar proteins and proteoglycans, which provide support for surrounding cells within most mammalian tissues and organs including exocrine glands. Although the comparative anatomy, histology and matrix composition of SGs has been studied extensively (Phang and Rannie, 1982; Lorber, 1992; Kamada et al., 1996; Macauley et al., 1997), the characterization of the LG ECM has received far less attention. Presently, only a few reports on LG histomorphology focusing on collagen, elastin or GAG are available (Alexander et al. 1973; Cherrick, 1975; Lorber, 1989; Sakai, 1989; Yoshida et al., 1996; Paulsen et al., 1998; Hosoyamada and Sakai, 2003; Pinard et al., 2003). A detailed analysis of the matrix structure in combination with a qualitative matrix protein evaluation has not been thoroughly documented in these publications.

This study represents the first comprehensive identification and characterization of the composition of LG ECM. Using routine technologies including histological, biochemical, immunohistochemical and gene expression analyses, we could demonstrate that healthy murine LGs are composed of collagen types I, III, and IV; elastin and tropoelastin; fibronectin; laminin 1; as well as glycoproteins including tenascin C, HS-GAG and decorin. For the first time, multiphoton-induced autofluorescence and SHG imaging were successfully applied for the analysis of unprocessed, fresh exocrine tissues without the need for any fixation or invasive processing. Using these powerful technologies we could assess collagenous and elastic fibers while maintaining the structural integrity of the assayed samples in their native state (Schenke-Layland et al., 2006). Moreover, taking advantage of routing methodologies combined with these novel imaging modalities we identified that an increased degradation of LG ECM structures including collagen, elastin and GAG is implicated in the pathogenesis of SS, representing a key event as the disease progresses.

SS is one of the three most common chronic autoimmune disorders (Pillemer et al., 2001). Despite extensive molecular, histological and clinical studies, the underlying cause of SS, its genetics and pathogenesis, remain largely unknown. It has been previously reported that glandular destruction in SS is mainly mediated by CD4-expressing T lymphocytes; however, an impaired secretory function of salivary and lacrimal glands in SS patients appears already in the initial phase of the inflammatory infiltration (Xanthou et al., 1999; Garcia-Carrasco et al., 2006). Using LGs of NOD mice, an established model to investigate many aspects of SS, we could reveal the presence of various subtypes of macrophages, neutrophilic and eosinophilic granulocytes, as well as B- and T-cells within the inflammatory cells that infiltrate the glandular tissues of the mice starting by 7 weeks of age. Furthermore, we detected a significant increase in MMP2 and MMP9 expression in NOD LGs as the disease progresses, predominantly appearing in areas of inflammation. This MMP up-regulation has been previously seen in NOD mouse SGs (Yamachika et al., 1998) and human SGs (Perez et al., 2000; Goicovich et al., 2003; Molina et al., 2006). Most interestingly, we further identified that the inflammatory infiltration of the glands was accompanied by a severe loss of normal LG ECM structure. Particularly, multiphoton imaging and SHG microscopy allowed an artifact-free, non-destructive tissue state evaluation of the unprocessed BALB/c and NOD LG tissues showing the disorganization and destruction of ECM structures including collagenous and elastic fibers. Compared to BALB/c LGs, only weak autofluorescent structures were visible within the NOD LG samples when exposed to laser pulses at 760 nm and especially at 840 nm. Spectral fingerprinting, which served as a quantitative measure of structural preservation or damage of intra-tissue collagen fibers, demonstrated that intrinsic SHG signals were almost non-detectable in NOD LGs. Immunohistochemical staining, as well as biochemical and gene expression analysis additionally supported these findings, showing an alteration of most of the ECM protein staining patterns in LGs of NOD mice when compared to BALB/c LG tissues, decreased protein contents and down-regulated gene expression.

It is possible that LG ECM damage is a primary process associated with SS due to fundamental changes in MMP expression and secretion from exocrine epithelial cells that weaken the tissue structures and therefore allow an infiltration of MMP-secreting inflammatory cells. Within this context, it is interesting that the increased tissue expression of MMPs was accompanied by decreased tissue gene expression of most ECM proteins, suggesting that changes in gene expression in the LG acinar cells contribute to creation of an environment ripe for inflammatory infiltration prior to the actual infiltration of immune cells. It is also possible that another event initiates LG invasion by infiltrating inflammatory cells that secrete MMPs, which causes ECM destruction, and that the apparent changes in gene expression play a more subtle role in the observed damage to ECM structures relative to the consequence of MMP expression. As well, the down-regulation of ECM gene expression detected in the LG in this scenario could represent an adaptive response in response to signals provided by the infiltrating immune cells by the gland. To determine the initial mechanistic events responsible for LG ECM degradation, we are currently conducting further studies using LG tissues of NOD/scid mice, as suggested by previous reports on SG tissues (Yamachika et al., 1998). Nevertheless, it is known that the infiltrating cells in SG interfere with the glandular function in several points including the production of autoantibodies, and the secretion of cytokines and MMPs, contributing to the disease progression (Garcia-Carrasco et al., 2006). Furthermore, it has been shown that the expression and regulation of MMPs in immune cells is necessary for the cell movement from blood to the ECM at all stages, including activation, homing to specific tissues, binding to endothelial cells, adhesion to and selective degradation of the ECM (Vaday and Lider, 2000). For example, T lymphocytes produce MMP2 and MMP9, which facilitate their migration through connective tissues; whereas macrophages secrete a wide range of MMPs that contribute to the remodeling of connective tissues, causing an alteration of the composition of the extracellular network that surrounds cells (Goetzl et al., 1996). However, there is increased evidence that acinar and ductal cells from SG of SS patients display a molecular potential, with increased capacity to markedly disorganize their ECM environment, damage their histoarchitecture and impair their functionality due to an increased MMP activity (Perez at al., 2000; Goicovich et al., 2003). Further investigations will be necessary to evaluate whether the finding that metabolic alteration in the exocrine cells themselves leads to the development of the SS pathology in SGs is also true for the progression of SS in LGs.

It should also be mentioned that in a mouse experimental model for dry eye involving desiccating stress, increased MMP9 activity has been confirmed in tear fluid washings (Luo et al., 2004), suggesting that MMPs may play a general role in inflammatory disorders in the ocular surface as well as those which are specifically associated with the autoimmune disease, SS, which affects the LG. Interestingly, the increased MMP9 expression was confirmed, at least in part, to be of corneal epithelial cell origin (Corrales et al., 2006).

The data shown here represent, to our knowledge, the most comprehensive study of the composition of LG ECM structures conducted to date. Using a variety of established routine and novel technologies we have qualitatively and quantitatively identified, characterized, and analyzed the ECM of healthy and diseased exocrine tissues. Our results clearly show an increased secretion of MMPs accompanied with an enhanced degradation of ECM proteins, as well as the severe disorganization and deformation of ECM structures of diseased LG tissues. At the current time, most therapeutic regimens for SS include a palliative component to treat the discomfort associated with loss of moisture production by the LG and SG, and an immunomodulatory component in an attempt to control the inflammatory responses directed at these tissues. Like other autoimmune diseases, the immunomodulatory therapies used for SS are not largely tissue-targeted to LG or SG and thus have systemic effects within the body. These therapies are designed to halt or delay the progression of the disease, rather than to target any specific processes that play a role in disease initiation. This limitation is largely due to the

fact that molecular events involved in disease initiation and progression are still poorly understood.

A clinical association between high levels of MMP expression and autoimmune diseases in general is established. MMP9 in particular has been implicated in disease processes ranging from lupus, SS, systemic sclerosis, rheumatoid arthritis, multiple sclerosis and atherosclerosis (Ram et al., 2006), although in many cases the observation of increased expression is correlative and its role in disease progression is unclear. In SS, MMP9 elevation was noted in SG biopsies and in saliva from SS patients (Konttinnen et al., 1998). In addition, higher MMP9 levels were seen in patients with primary SS, the more severe variant of the disease (Hulkkonen et al., 2004). In one study, an attempt to treat NOD mice with a general MMP inhibitor, as a preventive measure to block the observed lymphocytic infiltration and loss of SG function, was unsuccessful (Yamachika et al., 1998). However, other studies in a mouse model of systemic lupus erythematosus, utilizing a peptide derived from a novel anti-DNA antibody that specifically reduced plasma and kidney MMP activity, delayed the progression of the disease (Faber-Elmann et al., 2002). Clearly, there is much more to be done in animal models, including the NOD mouse used here, to explore the possibility that MMPs might represent therapeutic targets for SS. MMP expression, secretion, activation from the pro-enzyme form by proteases and endogenous mechanisms of inhibition are highly complex, and any of these points of regulation might represent a viable therapeutic target. Our observations that gene expression of ECM proteins are significantly reduced in LG in this SS experimental model adds a further dimension and identifies an additional series of potential therapeutic targets that might be amenable to modification.

4. Experimental Procedures

4.1. Animals

This study was conducted using LGs from male BALB/c (Jackson Labs, Bar Harbor/ME, USA) and NOD (Taconic Farms, Germantown/NY, USA) mice at the age of 7, 18 and 24 weeks. The mice were maintained in the USC vivarium facility on a 12-hour light-dark cycle and given food and water *ad libitum*. Animals were narcotized with a mixture of ketamine and xylazine and sacrificed with carbon dioxide. Careful visual inspection of the LGs was performed before and after removal. All procedures conformed to the standards and procedures for the proper care and use of animals in accordance with the institutional guidelines, and as described in the Declaration of Helsinki and the Guiding Principles in the Care and Use of Animals (DHEW publication, NIH 80-23).

4.2. Routine histology and immunohistochemistry

For routine histological and immunohistochemical analysis horizontal cryo-sections (5-8 μm) of LGs of 7, 18 and 24 weeks old BALB/c and NOD mice were cut, and processed according to previously described protocols (Schenke-Layland et al., 2005). All specimens were treated and sectioned similarly. Each tissue considered for histological analysis was stained with hematoxylin-eosin, a modification of Hart's resorcin–fuchsin stain (Starcher et al., 2005), or a modified Movat-pentachrome stain (Russell, 1972). After histological staining, all sections were mounted using Entellan (Electron Microscopy Sciences, Hatfield/PA, USA), analyzed and documented using routine bright-field light microscopy (Zeiss Axiovert 200 microscope, Carl Zeiss MicroImaging Inc., Thornwood/NY, USA).

Immunohistochemical staining was carried out as previously described (Schenke-Layland et al., 2007). Images were acquired using a confocal TCS SP2 AOBS laser-scanning microscope system (Leica Microsystems Inc., Exton/PA, USA) with 40x (1.3 numerical aperture (NA))

and 63x (1.4 NA) oil-immersion objectives, and processed with Adobe Photoshop 7.0 (Adobe Systems Inc., San Jose/CA, USA).

4.3. Antibodies

Primary antibodies used in this study include: I) polyclonal antibodies against fibronectin (A0245, 1:400; DAKO North America Inc., Carpinteria/CA, USA); collagen type I (R1038, 1:50; Novus Biologicals, Inc., Littleton/CO, USA); collagen type III (R1040, 1:50; Novus Biologicals, Inc.); collagen type IV (ab6586, 1:100; Abcam Inc., Cambridge/MA, USA); tropoelastin (ab21601, 1:100; Abcam Inc.); laminin 1 (ab11575, 1:50; Abcam Inc.); decorin (AF1060, 1:50; R&D Systems Inc., Minneapolis/MN, USA); MMP9 (AF-909, 1:50; R&D Systems Inc.); and alpha-smooth muscle actin (SMA, ab5694, 1:400; Abcam Inc.); as well as II) monoclonal antibodies against heparan-sulphated proteoglycans (ab2501, 1:100; Abcam Inc.); MMP2 (MAB3308, 1:1000; Chemicon); CD31 (PECAM-1) (550274, 1:50; BD Biosciences/Pharmingen, San Diego/CA, USA); CD4 (YTS191.1, 1:50; Serotec Inc., Raleigh/NC, USA), CD11b (Mac-1) (ab6332, 1:200; Abcam Inc.) and CD68 (FA-11, 1:50; Serotec Inc.).

Secondary antibodies included Alexa Fluor 488-conjugated goat-anti rabbit IgG (H+L), goat-anti rat IgG (H+L), goat-anti mouse IgG (H+L), and donkey-anti goat IgG (H+L); Alexa Fluor 594-conjugated goat-anti rat IgG (H+L); and Alexa Fluor 647-conjugated goat-anti rabbit IgG (H+L) (1:250; all from Invitrogen/Molecular Probes, Eugene/OR, USA).

4.4. Multiphoton imaging and SHG microscopy

Untreated LG cryo-sections or fresh dissected LGs of 18 weeks old BALB/c and NOD mice were examined using the Zeiss LSM 510 META NLO femtosecond laser scanning system mounted on an inverted Zeiss Axiovert 200M microscope (Carl Zeiss MicroImaging Inc.) and coupled to a software-tunable Coherent Chameleon titanium: sapphire laser (720 nm – 930 nm, 90 MHz; Coherent Laser Group, Santa Clara/CA, USA). The imaging system was equipped with a high-resolution AxioCam HRc camera with 1300 X 1030 pixels (Carl Zeiss MicroImaging Inc.). Images were collected using an oil immersion Plan-Neofluar 40x/1.3 numerical aperture DIC objective lens (Carl Zeiss MicroImaging Inc.). All observations were made using unprocessed, untreated intact tissues or fresh-frozen cryo-sections. For imaging of intact LGs, tissues were excised and placed in 35 mm glass-bottom dishes (MatTek Corporation, Ashland/MA, USA). Cellular and ECM structure-dependent autofluorescence, as well as SHG were induced using wavelengths of 740 nm (elastin, cells) and 860 nm (collagen). Non-invasive serial optical horizontal sections of four different areas of each of the specimens were taken in z-steps of 1 μm, 2 μm or 5 μm to depths of 20-50 μm. A band-pass (BP) 390-465 nm infrared-blocked filter and a short-pass (KP) 685 nm filter served as emission filters (Chroma Technology Corp, Rockingham/VT, USA). For maximum detection efficiency the pinhole was set to the maximum (1000 μm). All images were taken with a frame size of 512 × 512 pixels, with a pixel depth of 12-bit.

4.5. Spectral Fingerprinting

To quantify and compare the intrinsic fluorescence signals of elastic and collagenous structures within LG tissues of BALB/c and NOD mice, lambda stacks were ascertained at emission wavelengths of 390 nm to 520 nm (in 10 nm increments) using the two-photon Chameleon laser tuned to an excitation wavelength of either 740 nm or 860 nm. Emission was collected using the Zeiss META detector (spectral separator) of the LSM 510 Meta NLO system. The scans were acquired with a scan time of 2.56 μs/pixel, 8 times summarization to enhance the signal, in plane multi track 8-bit lambda mode, and analyzed by the Zeiss AIM version 3.2 software (Carl Zeiss MicroImaging Inc.). Due to a reproducible laser excitation power and similar exposure times for all samples, mean intensities of the intrinsic fluorescence signals

were calculated and used for quantification. In each case, 6 different areas of each tissue sample were scanned and intensities of the intrinsic fluorescence signals of the regions of interest (ROI; equals the area of the highest intensity) were detected. The signal intensities were reflected by the gray values of all the pixels within a ROI (gray value intensities (GVI)). Mean intensities were calculated from the screened ROI areas. Accordingly, all results are presented as mean values ± standard deviations (SD).

4.6. RNA extraction, cDNA synthesis, RT-PCR and real-time RT-PCR

Total RNA was extracted from LGs of BALB/c and NOD mice (n=4 each; age: 18 weeks), as well as from adult BALB/c mouse kidney and lung tissues (served as controls) using the Versagene RNA tissue kit (Gentra Systems, Inc., Minneapolis/MN, USA) and treated with DNase (Versagene Dnase treatment kit, Gentra Systems, Inc.) as per the manufacturer's instructions. First strand cDNA was generated from 2 μg of total RNA by using the Omniscript™ Reverse Transcriptase Kit (Qiagen, Valencia/CA, USA) as per manufacturer's instructions. All samples, along with the corresponding “no-RT” control (RNA) to confirm the absence of contaminating genomic DNA, were subjected to PCR (for each primer n=4), carried out using 2.5 units of Taq DNA Polymerase, 10x PCR buffer, 2.5 mM $MgCl_2$, 200 μM dNTPs, Q-solution, and specific primers (all from Qiagen). The collagen type I (Col1a1, Col1a2), type III (Col3a1) and type IV (Col4a1), laminin 1 (Lama1), decorin (Dcn), tenascin C (Tnc), and elastin (Eln) primer sets were obtained from Qiagen (QuantiTect Primer Assay) and used according to the manufacturer's instructions. Primer sets for RAB3D member RAS oncogene family (Rab3d) (specifically expressed in lacrimal acini cells (da Costa et al., 2006)), phosphoglycerate kinase 1 (Pgk1) and glyceraldehyde-3-phosphate dehydrogenase (Gapdh) (all Qiagen) were used as internal controls. The resultant PCR products were resolved through 2.5% agarose gels stained with ethidium bromide.

Real-time PCR was conducted using the ABI PRISM 7700 Sequence Detection System, Taqman (Applied Biosystems, Foster City/CA, USA) (n=4). Primer sets utilized for real-time quantification were the same primer sets used for semi-quantitative RT-PCR, obtained from Qiagen and used following the manufacture's instructions. PCR amplicons were detected by fluorescent detection of SYBR Green (QuantiTect SYBR Green PCR Kit, Qiagen). Cycling conditions were as follows; 95°C for 15 min followed by 40 cycles at 94°C for 15 sec, 55°C for 30 sec and 72°C for 30 sec.

4.7. Biochemical analyses

Biochemical assays were used for the quantitative analysis of ECM components of a representative number of BALB/c and NOD LG tissues (each n=14 glands (7 animals; age: 18 weeks)). Crude tissue lysates were prepared using a homogenizer and buffers as described previously (Stock et al., 2001). All samples were normalized according to their wet weight in mg. Total collagen and GAG contents were quantified using SIRCOL and BLYSCAN assays (Biocolor, Belfast, Northern Ireland) as per manufacturer's instructions. The desmosine content in BALB/c and NOD LG tissues (each n=14 glands (7 animals)) was determined using a radioimmunoassay as described in detail elsewhere (Starcher and Conrad, 1995).

4.8. Gelatinase activity assay

Total protein from LGs of 18 weeks old BALB/c and NOD mice was extracted in 10 mM Tris, pH 7.4/150 mM NaCl/1 mM $CaCl_2$/1 mM $MgCl_2$/0.1% Triton X-100, in the presence of the protease inhibitor mixture Complete Mini (Roche Diagnostics GmbH, Mannheim, Germany) (Rodríguez-Manzaneque et al., 2001). The protein content was determined by a colorimetric assay (Bio-Rad, Hercules/CA, USA). For the evaluation of gelatinase A (MMP2) and B (MMP9) activity in BALB/c and NOD LG tissues, we used the MMP-Gelatinase Activity

Assay Kit (Chemicon) according to the manufacture's instructions and as previously described (Rodríguez-Manzaneque et al., 2001; Brown et al., 2004).

4.9. Flow cytometric analysis

FACS analysis was performed on inflammatory cells, which were isolated from 18 glands of 9 NOD mice according to a modified protocol as described previously (Guo et al., 2000). In order to identify the proportions of macrophages; neutrophils and eosinophils; as well as T- and B-cells, cells were dual-stained with the following antibodies: cyanine-5 (Cy5)-conjugated CD11b (Mac-1) and phycoerythrin (PE)-conjugated Gr1; PE-conjugated B220 and fluorescein isothiocyanate (FITC)-conjugated CD19; as well as FITC-conjugated CD4 and PE-conjugated CD8 (all purchased from BD Biosciences/Pharmingen) according to the manufacturer's protocol. Nonspecific isotype-matched Cy5-, PE- and FITC-conjugated IgGs served as controls. All analyses were performed using a BD LSR2 flow cytometer (BD Bioscience, San Jose/CA, USA). FCS files were exported and analyzed using the FlowJo 8.3.3 software (Tree Star Inc., Ashland/OR, USA).

4.10. Statistics

All results are presented as mean values ± standard deviation. Significant differences between BALB/c and NOD LG tissues were assessed by ANOVA with Tukey's multiple comparison test and Student's *t* test. *P*-values less than 0.05 were defined as statistically significant.

Acknowledgements

The authors would like to thank Michelle Mac Veigh for her excellent technical assistance with the histology; as well as Katrin E. Rhodes, Ben Van Handel and Matthias Magnusson for helpful discussions on the FACS data. This work was supported by the Deutsche Forschungsgemeinschaft (DFG; Sche701/2-1) and gifts from the Laubisch and Glazer Funds (K.S-L.); NIH R01HL70748 and AHA 0340087N (W.R.M.); and NIH EY-11386, EY -16985 and EY-17293 (S.H-A.).

References

Alexander JH, Young JA, van Lennep EW. The ultrastructure of the duct system in the rat extraorbital lacrimal gland. Z Zellforsch 1973;144:453–466. [PubMed: 4793164]

Brown DJ, Lin B, Chwa M, Atilano SR, Kim DW, Kenney MC. Elements of the nitric oxide pathway can degrade TIMP-1 and increase gelatinase activity. Mol Vis 2004;10:281–288. [PubMed: 15105792]

da Costa SR, Wu K, Pidgeon M, Ding C, Schechter JE, Hamm-Alvarez SF. Male NOD mouse external lacrimal glands exhibit profound changes in the exocytotic pathway early in postnatal development. Exp Eye Res 2006;82(1):33–45. [PubMed: 16005870]

Cherrick HM. The histomophologic and histochemical evaluation of the salivary and exorbital lacrimal glands in the hairless mouse. J Oral Med 1975;30:24–28. [PubMed: 45939]

Corrales RM, Stern ME, De Paiva CS, Welch J, Li DQ, Pflugfelder SC. Dessicating stress stimulates production of matrix metalloproteinases by the corneal epithelium. Invest Ophthal Vis Sci 2006;47:3297–3302.

Cowan KN, Jones PL, Rabinovitch M. Elastase and matrix metalloproteinase inhibitors induce regression, and tenascin-C antisense prevents progression, of vascular disease. J Clin Invest 2000;105:21–34. [PubMed: 10619858]

Faber-Elmann A, Eilat E, Zinger H, Mozes E. A peptide based on an anti-DNA autoantibody downregulates matrix metalloproteinases in murine models of lupus. Clin Immunol 2002;105:223–232. [PubMed: 12482397]

Fox RI, Adamson TC 3rd, Fong S, Robinson CA, Morgan EL, Robb JA, Howell FV. Lymphocyte phenotype and function of pseudolymphoma associated with Sjögren's syndrome. J Clin Invest 1983;72:52–59. [PubMed: 6603476]

Fox RI, Robinson CA, Curd J, Kozin F, Howell FV. Sjögren's syndrome: proposed criteria for classification. Arthritis Rheum 1986;29:577–585. [PubMed: 3718551]

Garcia-Carrasco M, Fuentes-Alexandro S, Escarcega RO, Salgado G, Riebeling C, Cervera R. Pathophysiology of Sjögren's Syndrome. Arch Med Res 2006;37:921–932. [PubMed: 17045106]

Germain RN. T-cell development and the CD4-CD8 lineage decision. Nat Rev Immunol 2002;2(5):309–322. [PubMed: 12033737]

Goetzl EJ, Banda MJ, Leppert D. Matrix metalloproteinases in immunity. J Immunol 1996;156:1–4. [PubMed: 8598448]

Goicovich E, Molina C, Perez P, Aguilera S, Fernandez J, Olea N, Alliende C, Leyton C, Romo R, Leyton L, Gonzalez MJ. Enhanced degradation of proteins of the basal lamina and stroma by matrix metalloproteinases from the salivary glands of Sjogren's syndrome patients: correlation with reduced structural integrity of acini and ducts. Arthritis & Rheumatism 2004;48(9):2574–2584.

Guo Z, Azzarolo AM, Schechter JE, Warren DW, Wood RL, Mircheff AK, Kaslow HR. Lacrimal gland epithelial cells stimulate proliferation in autologous lymphocyte preparations. Exp Eye Res 2000;71(1):11–22. [PubMed: 10880272]

Hosoyamada Y, Sakai T. The ultrastructure of periductal connective tissue and distinctive populations of collagen fibrils associated with ductal epithelia of exocrine glands. Arch Histol Cytol 2003;66:407–418. [PubMed: 15018143]

Hulkonnen J, Pertovaara M, Antonen J, Pasternack A, Hurme M, Pollanen P, Lehtimaki T. Matrix metalloproteinase 9 (MMP-9) gene polymorphism and MMP-9 levels in primary Sjogren's symdrome. Rheumatol 2004;43:1476–1479.

Humphreys-Beher MG, Peck AB. New concepts for the development of autoimmune exocrinopathy derived from studies with the NOD mouse model. Arch Oral Biol 1999;44:S21–25. [PubMed: 10414851]

Imanaka-Yoshida K, Matsumoto K, Hara M, Sakakura T, Yoshida T. The dynamic expression of tenascin-C and tenascin-X during early heart development in the mouse. Differentiation 2003;71(45):291–298. [PubMed: 12823230]

Kamada A, Tamura I, Okazaki J, Matsukawa F, Sakai T. Characteristics and localization of rat submandibular gland proteoglycans. Arch Oral Biol 1996;41:951–958. [PubMed: 9031702]

Kostianovsky M, Greco MA, Cangiarella J, Zagzag D. Tenascin-C expression in ultrastructurally defined angiogenic and vasculogenic lesions. Ultrastruct Pathol 1997;21(6):537–544. [PubMed: 9355236]

Konttinnen YT, Halinen S, Hanemaaijer R, Sorsa T, Hietanen J, Ceponis A, Xu JW, Manthorpe R, Whittington J, Larsson A, Sali T, Kjeltsen L, Stenman UH, Eisen AZ. Matrix metalloproteinase (MMP)-9 type IV collagenase/gelatinase implicated In the pathogenesis of Sjogren's symdrome. Matrix Biol 1998;17:335–347. [PubMed: 9822200]

Kusmartsev SA, Li Y, Chen SH. Gr-1 myeloid cells derived from tumor-bearing mice inhibit primary T cell activation induced through CD3/CD28 costimulation. J Immunol 2000;165:779–785. [PubMed: 10878351]

Lorber M. Elastic fibers in the rat exorbital lacrimal gland duct system. Invest Ophtalmol Vis Sci 1989;30:2002–2011.

Lorber M. Elastic fibers in the duct system of the rat submandibular salivary gland. Anat Rec 1992;234:335–347. [PubMed: 1443662]

Luo L, Li DQ, Doshi A, Farley W, Corrales RM, Pflugfelder SC. Experimental dry eye stimulates production of inflammatory cytokines and MMP-9 and activates MAPK signaling pathways on the ocular surface. Invest Ophthal Vis Sci 2004;45:4293–4301. [PubMed: 15557435]

Macauley SP, Tarnuzzer RW, Schultz GS, Chegini N, Oxford GE, Humphreys-Beher MG. Extracellular-matrix gene expression during mouse submandibular gland development. Arch Oral Biol 1997;42:443–454. [PubMed: 9382709]

Maruyama K, Masaaki I, Cursiefen C, Jackson DG, Keino H, Tomita M, Van Rooijen N, Takenaka H, D'Amore PA, Stein-Streilein J, Losordo DW, Streilein JW. Inflammation-induced lymphangiogenesis in the cornea arises from CD11b-positive macrophages. J Clin Invest 2005;115(9):2363–2372. [PubMed: 16138190]

Matsumoto I, Tsubota K, Satake Y, Kita Y, Matsumura R, Murata H, Namekawa T, Nishioka K, Iwamoto I, Saitoh Y, Sumida T. Common T Cell Receptor Clonotype in Lacrimal Glands and Labial Salivary Glands from Patients with Sjögren's Syndrome. J Clin Invest 1996;97(8):1969–1977. [PubMed: 8621782]

Molina C, Alliende C, Aguilera S, Kwon YJ, Leyton L, Martinez B, Leyton C, Perez P, Gonzalez MJ. Basal lamina disorganization of the acini and ducts of labial salivary glands from patients with Sjögren's syndrome: association with mononuclear cell infiltration. Ann Rheum Dis 2006;65:178–183. [PubMed: 16014676]

Ogawa M, ten Boekel E, Melchers F. Identification of $CD19^{-}B220^{+}$c-$Kit^{+}Flt3/Flk\text{-}2^{+}$cells as early B lymphoid precursors before pre-B-I cells in juvenile mouse bone marrow. Int Immunol 2000;12(3): 313–324. [PubMed: 10700466]

Paulsen F, Thale A, Kohla G, Schauer R, Rochels R, Parwaresch R, Tillman B. Functional anatomy of human lacrimal duct epithelium. Anat Embryol 1998;198:1–12. [PubMed: 9683063]

Perez P, Goicovich E, Alliende C, Aguilera S, Leyton C, Molina C, Pinto R, Romo R, Martinez B, Gonzalez MJ. Differential expression of matrix metalloproteinases in labial salivary glands of patients with primary Sjogren's symdrome. Arthritis & Rheumatism 2000;43(12):2807–2817. [PubMed: 11145040]

Phang YC, Rannie I. Oxytalan and elastic fibres in human salivary glands. A light microscopy study. Aust Dent J 1982;27:288–290. [PubMed: 6962691]

Pillemer SR, Matteson EL, Jacobsson LT, Martens PB, Melton LJ 3rd, O'Fallon WM, Fox PC. Incidence of physician-diagnosed primary Sjogren syndrome in residents of Olmsted County. Minnesota Mayo Clin Proc 2001;76:593–599.

Pinard CL, Weiss ML, Brightman AH, Fenwick BW, Davidson HJ. Normal anatomical and histochemical characteristics of the lacrimal glands in the American bison and cattle. Anat Histol Embryol 2003;32:257–262. [PubMed: 12969024]

Qian L, Xie J, Rose CM, Sou E, Zeng H, Hamm-Alvarez SF, Mircheff AK. Altered traffic to the lysosome in an ex vivo lacrimal acinar cell model for chronic muscarinic receptor stimulation. Exp Eye Res 2004;79(5):665–675. [PubMed: 15500825]

Qian L, Wang Y, Xie J, Rose CM, Yang T, Nakamura T, Sandberg M, Zeng H, Schechter JE, Chow RH, Hamm-Alvarez SF, Mircheff A. Biochemical changes contributing to functional quiescence in lacrimal gland acinar cells after chronic ex vivo exposure to a muscarinic agonist. Scand J Immunol 2003;58(5):550–565. [PubMed: 14629627]

Ram M, Sherer Y, Shoenfeld Y. Matrix Metalloproteinase-9 and autoimmune disease. J Clin Immunol 2006;26:299–306. [PubMed: 16652230]

Rodríguez-Manzaneque JC, Lane TF, Ortega MA, Hynes RO, Lawler J, Iruela-Arispe ML. Thrombospondin-1 suppresses spontaneous tumor growth and inhibits activation of matrix metalloproteinase-9 and mobilization of vascular endothelial growth factor. Proc Natl Acad Sci USA 2001;98(22):12485–12490. [PubMed: 11606713]

Robinson CP, Yamachika S, Alford CE, Cooper C, Pichardo EL, Shah N, Peck AB, Humphreys-Beher MG. Elevated levels of cysteine protease activity in saliva and salivary glands of the nonobese diabetic (NOD) mouse model for Sjogren's syndrome. Proc Natl Acad Sci USA 1997;94(11):5767–5771. [PubMed: 9159148]

Rose CM, Qian L, Hakim L, Wang Y, Jerdeva GY, Marchelletta R, Nakamura T, Hamm-Alvarez SF, Mircheff AK. Accumulation of catalytically active proteases in lacrimal gland acinar cell endosomes during chronic ex vivo muscarinic receptor stimulation. Scand J Immunol 2005;61(1):36–50. [PubMed: 15644121]

Russell HK Jr. A modification of Movat's pentachrome stain. Arch Pathol 1972;94:187–191. [PubMed: 4114784]

Sakai T. Major ocular glands (harderian gland and lacrimal gland) of the musk shrew (Suncus murinus) with a review on the comparative anatomy and histology of the mammalian lacrimal glands. J Morphol 1989;210:39–57. [PubMed: 2664187]

Schenke-Layland K, Riemann I, Stock UA, König K. Imaging of cardiovascular structures using near-infrared femtosecond multiphoton laser microscopy. J Biomed Opt 2005;10(2):024017. [PubMed: 15910091]

Schenke-Layland K, Riemann I, Damour O, Stock UA, König K. Two-photon microscopes and *in vivo* multiphoton tomographs--powerful diagnostic tools for tissue engineering and drug delivery. Adv Drug Deliv Rev 2006;58:878–896. [PubMed: 17011064]

Schenke-Layland K, Angelis E, Rhodes KE, Heydarkhan-Hagvall S, Mikkola HK, MacLellan WR. Collagen IV induces trophoectoderm differentiation of mouse embryonic stem cells. Stem Cells 2007;25(6):1529–1538. [PubMed: 17363553]

Schlüter OM, Khvotchev M, Jahn R, Südhof TC. Localization versus function of Rab3 proteins. Evidence for a common regulatory role in controlling fusion. J Biol Chem 2002;277(43):40919–40929. [PubMed: 12167638]

Sjögren H. Zur Kenntnis Keratoconjunctivitis sicca. Acta Ophthalmol 1933;2:1–151.

Starcher B, Conrad M. A role for neutrophil elastase in the progression of solar elastosis. Connect Tissue Res 1995;31:133–140. [PubMed: 15612329]

Starcher B, Aycock RL, Hill CH. Multiple Roles for Elastic Fibers in the Skin. J Histochem Cytochem 2005;53:431–443. [PubMed: 15805418]

Stock UA, Wiederschain D, Kilroy SM, Shum-Tim D, Khalil PN, Vacanti JP, Mayer JE Jr, Moses MA. Dynamics of extracellular matrix production and turnover in tissue engineered cardiovascular structures. J Cell Biochem 2001;81:220–228. [PubMed: 11241662]

Tsubota K, Xu K, Fujihara T, Katagiri S, Takeuchi T. Decreased reflex tearing is associated with lymphocytic infiltration in lacrimal glands. J Rheumatology 1996;23:313–320.

Tsubota K, Hirai S, King LS, Agre P, Ishida N. Defective cellular trafficking of lacrimal gland aquaporin-5 in Sjogren's syndrome. Lancet 2001;357(9257):2054–2055.

Vaday GG, Lider O. Extracellular matrix moieties, cytokines, and enzymes: dynamic effects on immune cell behavior and inflammation. J Leukoc Biol 2000;67:149–159. [PubMed: 10670574]

Xanthou G, Tapinos NI, Polihronis M, Nezis IP, Margaritis LH, Moutsopoulos HM. CD4 cytotoxic and dendritic cells in the immunopathologic lesion of Sjogren's syndrome. Clin Exp Immunol 1999;118:154–163. [PubMed: 10540173]

Yamachika S, Nanni JM, Nguyen KH, Garces L, Lowry MM, Robinson CP, Brayer J, Oxford GE, da Silveira A, Kerr M, Peck AB. Excessive synthesis of matrix metalloproteinases in exocrine tissues of NOD mouse models for Sjogren's syndrome. J Rheumatol 1998;25(12):2371–2380. [PubMed: 9858432]

Yoshida K, Nitatori Y, Uchiyama Y. Localization of glycosaminoglycans and CD44 in the human lacrimal gland. Arch Histol Cytol 1996;59:505–513. [PubMed: 9037387]

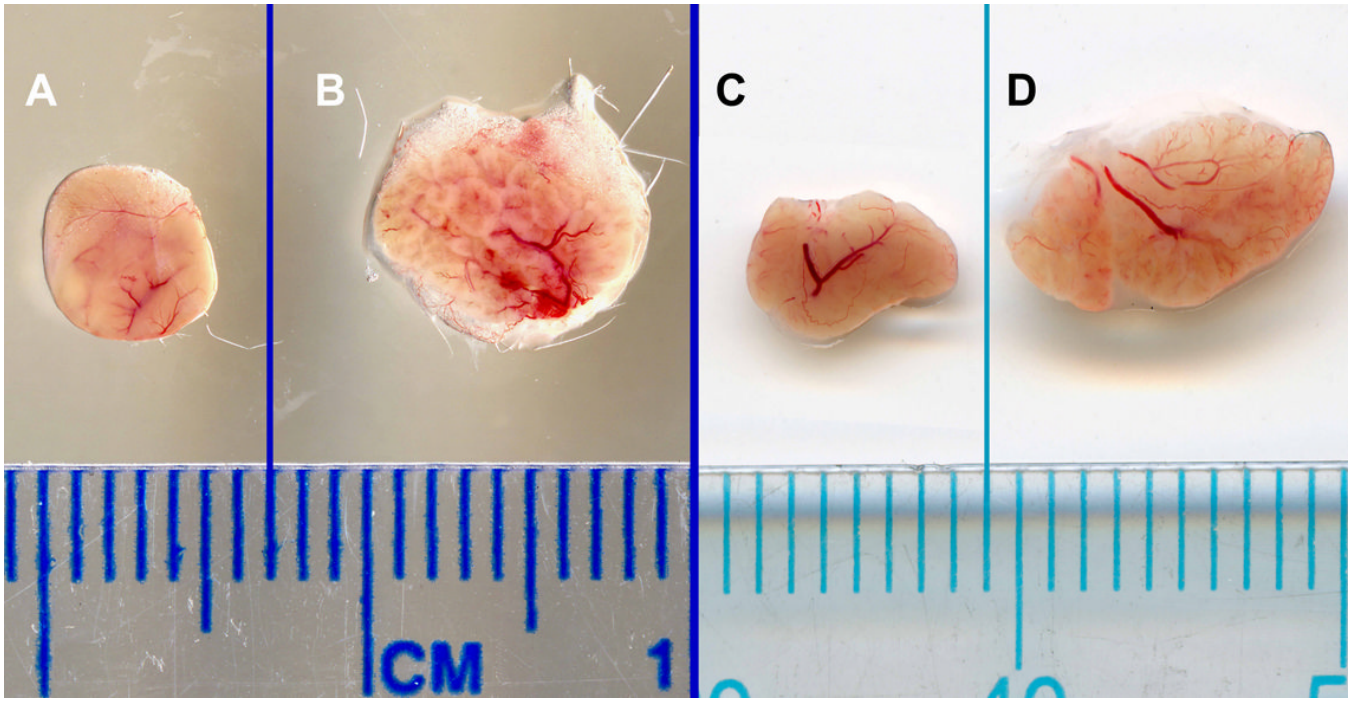

Fig. 1.
Photomicrographs of LGs dissected from age-matched, 18 (A, B) and 24 (C, D) week old BALB/c (A, C) and NOD (B, D) mice.

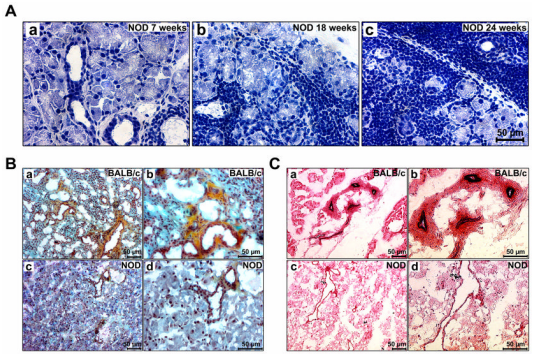

Fig. 2.

(A) Hematoxylin-eosin staining of LG sections of 7 (a), 18 (b), and 24 (c) weeks old NOD mice showing that with increasing age the acinar tissue sustains a severe inflammatory infiltration. (B) Movat-pentachrome staining of 18 weeks old BALB/c (a, b) and NOD (c, d) LGs. Collagen=yellow, GAG=blue-green, elastin=dark-blue/black, nuclei=dark-red. (C) When compared to Hart's stained BALB/c LG sections (a, b), the LG tissue of age-matched 18 week old NOD mice (c, d) shows less elastic fibers, with fewer, but enlarged ducts and blood vessels.

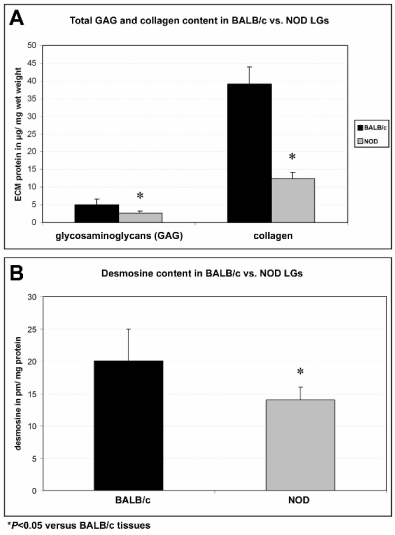

Fig. 3.

Biochemical analysis demonstrates a significant loss of ECM proteins including GAG, total collagen and desmosine in LG tissues of 18 weeks old NOD mice when compared to age-matched BALB/c tissues.

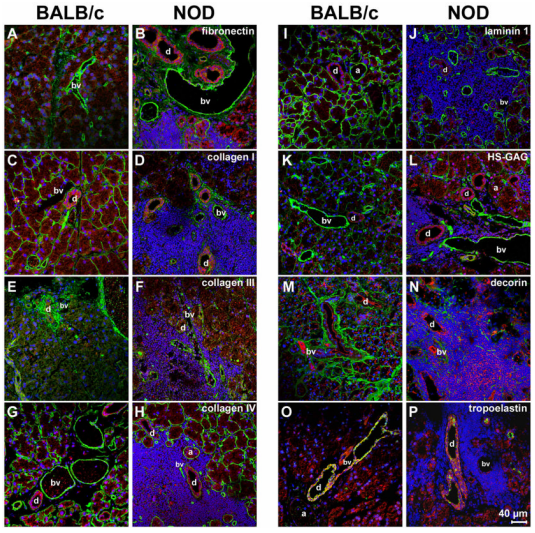

Fig. 4.

Immunohistochemical analysis of LGs of 18 weeks old NOD mice reveals massive inflammatory infiltrates, mainly located around the acini (a), blood vessels (bv) and ducts (d), associated with a spatial degradation of ECM proteins. Images show F-actin staining (red) as well as positive staining (green) for: fibronectin (A, B); collagen type I (C, D); collagen type III (E, F); collagen type IV (G, H); laminin 1 (I, J); HS-GAG (K, L); decorin (M, N); and tropoelastin (O, P). DAPI-staining was performed to show cell nuclei (blue).

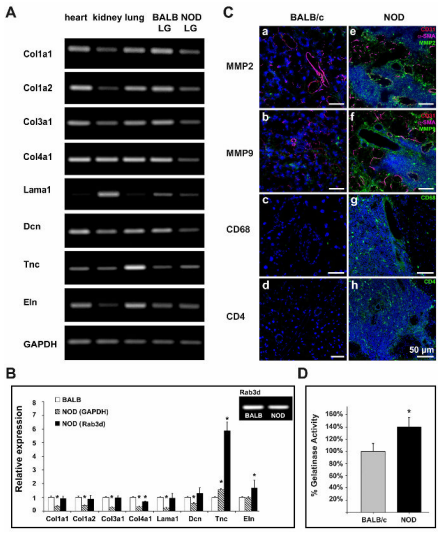

Fig. 5.

(A) Gene expression analysis of age-matched (18 weeks) NOD LGs compared to LG tissues of BALB/c mice showing a down-regulated expression of collagens I, III and IV, laminin 1, and decorin, as well as an increased expression of tenascin C in NOD LGs. No significant changes in elastin expression were noticed. (B) Real-time RT-PCR analysis (*-P<0.05 versus BALB/c), and Rab3d-expression pattern in BALB/c and NOD LGs. (C) Immunohistochemical staining reveals a dramatic up-regulation of MMP2 and MMP9 in areas of inflammation in NOD LG tissues (a-d versus e-h). Images show positive staining for MMP2 (a, e), MMP9 (b, f), CD68 (c, g) and CD4 (d, h) in green; endothelial cells (CD31) in red, and smooth muscle (SMA) in magenta (a, b, e, f); as well as cell nuclei (DAPI) in blue. (D) The gelatinase activity assay reveals a statistically significant increase of MMP2/9 activity in NOD LGs when compared to BALB LGs (*-P<0.05 versus BALB/c).

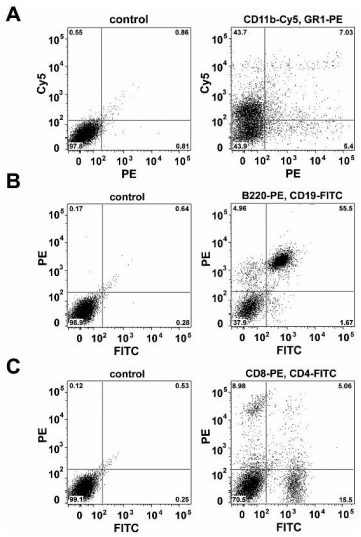

Fig. 6.

Dot-plot profiles of inflammatory infiltrates reveal the presence of clear populations of (A) macrophages as well as neutrophilic and eosinophilic granulocytes; (B) B-cells and (C) T-cells.

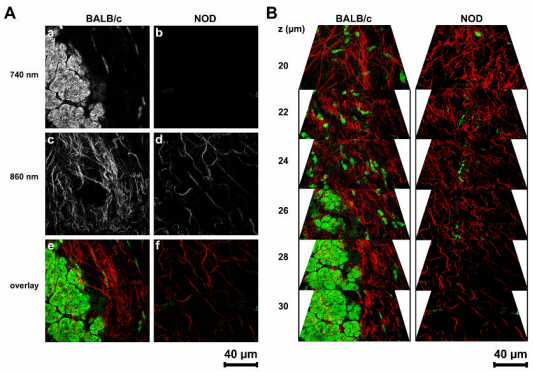

Fig. 7.

(A) Multiphoton-induced autofluorescence images of fresh dissected, untreated LGs of 18 weeks old BALB/c and NOD mice using two wavelengths of 740 nm (a, b; elastin and cells) and 860 nm (c, d; collagen). Images (e) and (f) represent an overlay of images (a; green) and (c; red), as well as (b; green) and (d; red). Please note that within NOD LG tissues almost no autofluorescence is detectable using a wavelength of 740 nm (b and f (green)). To induce autofluorescent structures at 860 nm a higher laser power is needed (d and f (red)). (B) Three-dimensional reconstruction of autofluorescence images of BALB/c and NOD LGs showing elastic fibers and predominantly cells in green, and collagenous structures in red.

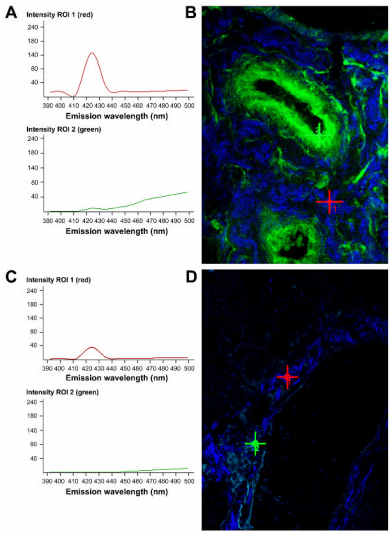

Fig. 8.

Spectral fingerprinting of BALB/c (A, B) and NOD (C, D) LG tissues using comparable laser powers and excitation wavelengths of 860 nm (ROI 1, red) and 740 nm (ROI 2, green). (A, C) The graphs represent peak SHG intensities of collagenous structures (ROI 1, red), as well as peak autofluorescence intensities of elastin-containing fibers and cells (ROI 2, green) in the corresponding lambda stack overlay image (B and D), denoted by the red (ROI 1) or the green (ROI 2) cross. (B, D) The red cross depicts the blue SHG signal of collagen emitting at about 425 nm. The green signal (green cross) at a peak emission wavelength of approximately 510 nm corresponds predominantly to elastic components. Note the aberrant, very faint NOD LG SHG signal (C and D), indicating a substantial ultrastructural deterioration and disintegration of most collagen fibers. Almost no signal for elastin-containing structures is detectable in NOD tissues.

Table 1

ECM protein expression intensity patterns in BALB/c and NOD LG tissues

ECM protein	acini		ducts		blood vessel	
	BALB/c	NOD	BALB/c	NOD	BALB/c	NOD
collagen type I	+++	-	+	(+)	+++	+++
collagen type III	+	-	+++	++	++	++
collagen type IV	+++	(+)	++	++	+++	+++
fibronectin	+	+	++	++	+++	+++
laminin 1	+++	-	+	+	+++	+++
HS-GAG	++	(+)	+	+	+++	+++
decorin	++	+	++	+	++	+
tropoelastin	-	-	+++	++	+	-

- no expression; (+) very weak expression; + weak expression; ++ expression; +++ strong expression